ADVANCED MATERIALS
www.advmat.de

Freestanding 3D Mesostructures, Functional Devices, and Shape-Programmable Systems Based on Mechanically Induced Assembly with Shape Memory Polymers

Xueju Wang, Xiaogang Guo, Jilong Ye, Ning Zheng, Punit Kohli, Dongwhi Choi, Yi Zhang, Zhaoqian Xie, Qihui Zhang, Haiwen Luan, Kewang Nan, Bong Hoon Kim, Yameng Xu, Xiwei Shan, Wubin Bai, Rujie Sun, Zizheng Wang, Hokyung Jang, Fan Zhang, Yinji Ma, Zheng Xu, Xue Feng, Tao Xie, Yonggang Huang, Yihui Zhang, and John A. Rogers**

Capabilities for controlled formation of sophisticated 3D micro/nanostructures in advanced materials have foundational implications across a broad range of fields. Recently developed methods use stress release in prestrained elastomeric substrates as a driving force for assembling 3D structures and functional microdevices from 2D precursors. A limitation of this approach is that releasing these structures from their substrate returns them to their original 2D layouts due to the elastic recovery of the constituent materials. Here, a concept in which shape memory polymers serve as a means to achieve freestanding 3D architectures from the same basic approach is introduced, with demonstrated ability to realize lateral dimensions, characteristic feature sizes, and thicknesses as small as ≈500, 10, and 5 μm simultaneously, and the potential to scale to much larger or smaller dimensions. Wireless electronic devices illustrate the capacity to integrate other materials and functional components into these 3D frameworks. Quantitative mechanics modeling and experimental measurements illustrate not only shape fixation but also capabilities that allow for structure recovery and shape programmability, as a form of 4D structural control. These ideas provide opportunities in fields ranging from micro-electromechanical systems and microrobotics, to smart intravascular stents, tissue scaffolds, and many others.

Complex 3D functional architectures are of widespread interest due to their potential applications in biomedical devices,[1–5] metamaterials,[6–10] energy storage and conversion platforms,[11–16] and electronics systems.[17–23] Although existing fabrication techniques such as 3D printing,[4,14,24–32] templated growth,[33–36] and controlled folding[2,37–43] can serve as powerful routes to diverse classes of 3D structures that address requirements in a number of interesting technologies, each has some set of limitations in materials compatibility, accessible feature sizes, and compatibility with well-developed 2D processing techniques used in the semiconductor and photonics industries.[44–46] Despite significant efforts in research and development, there remains a need for methods that provide access to complex 3D mesostructures that incorporate high-performance materials.

Dr. X. Wang, Dr. Y. Zhang, Q. Zhang, Dr. B. H. Kim, Y. Xu, Dr. W. Bai, H. Jang, Prof. J. A. Rogers
Simpson Querrey Institute and Feinberg Medical School
Center for Bio-Integrated Electronics
Northwestern University
Evanston, IL 60208, USA
E-mail: jrogers@northwestern.edu

Dr. X. Wang
Department of Mechanical and Aerospace Engineering
University of Missouri–Columbia
Columbia, MO 65211, USA

Dr. X. Guo, Dr. F. Zhang, Dr. Y. Ma, Z. Xu, Prof. X. Feng, Prof. Y. Zhang
Center for Mechanics and Materials
Center for Flexible Electronics Technology
Applied Mechanics Laboratory
Department of Engineering Mechanics
Tsinghua University
Beijing 100084, P. R. China
E-mail: yihuizhang@mail.tsinghua.edu.cn

J. Ye, State Key Laboratory of Tribology
Center for Nano and Micro Mechanics
Tsinghua University
Beijing 100084, P. R. China

N. Zheng, Prof. T. Xie
State Key Laboratory of Chemical Engineering
College of Chemical and Biological Engineering
Zhejiang University
Hangzhou 310027, P. R. China

Prof. P. Kohli
Department of Chemistry and Biochemistry
Southern Illinois University
Carbondale, IL 62901, USA

Dr. D. Choi
Department of Mechanical Engineering
Kyung Hee University
Yongin 17104, South Korea

DOI: 10.1002/adma.201805615

A collection of recent publications reports schemes that exploit compressive buckling as a means for assembly of complex 3D functional devices in a diversity of configurations and with a broad range of material compositions, including critical dimensions that span nanometer to centimeter length scales.[47–51] Here, relaxation of a prestrained elastomer substrate, as an assembly platform, imposes stresses on a 2D precursor structure to transform its geometry into a desired 3D shape. With a few exceptions,[52,53] deformations of the micro/nanomaterials in the precursor remain in the elastic range, partly to avoid damage or alterations in the properties of the constituent materials and partly to facilitate reproducibility in the transformation process and alignment with quantitative mechanics modeling of the process. A key disadvantage of operation in this elastic regime is that it frustrates the realization of freestanding 3D mesostructures, simply because they return to their original 2D shapes when released from the assembly platform. This feature sets limitations on practical applications for 3D systems in isolated forms (e.g., microrobotics) or in those that demand operation under conditions (e.g., elevated temperatures or precise dimensional stability) that are incompatible with the elastomer substrate. Recently reported approaches to address this problem rely on interfacial photopolymerization to form stable supporting platforms for the 3D structures or on nonlinear elastoplastic deformations in the constituent materials.[36] The resulting structures, however, are either confined to a base or they suffer from poor dimensional control due to a certain degree of recovery resulting from the elastic component of the deformations. The development of a robust, versatile technique to enable fully freestanding complex 3D mesostructures without such drawbacks remains a challenge.

The following reports a strategy that utilizes the shape fixation and memory effects associated with shape memory polymers (SMPs) to 1) enable freestanding 3D mesostructures and functional devices formed by compressive buckling in the elastic regime, 2) impart them with an ability to recover from severe deformations, and 3) change shape in a programmable fashion. The scheme begins with geometric transformation of 2D precursors formed in an SMP, with or without integrated functional materials, into 3D mesostructures using procedures similar to those described previously. Heating the resulting 3D mesostructures to temperatures above the glass transition temperature (T_{trans}) of the SMP followed by cooling to room temperature fixes the 3D shape, in a way that allows release from the assembly platform with no measurable change in geometry. This technique provides easy access to a broad range of 3D structures in SMPs with thicknesses in the micrometer range, and lateral sizes spanning microscale to centimeter scales, with features that would be difficult or impossible to reproduce using other methods. Integrating functional materials and electronic components onto the 2D precursor structures can result in freestanding 3D functional devices, as demonstrated in wirelessly controlled, battery-free light emitting systems. The capabilities introduced here provide unique opportunities for unusual applications in soft robotics, flexible electronics, medical devices, micro-electromechanical systems, and many others.

Figure 1a shows a schematic illustration of the process for forming 3D mesostructures in SMPs. The scheme begins with the microfabrication of a 2D pattern in a thin film of SMP made from a mixture of epoxy monomer (E44; China Petrochemical Corporation) and curing agent (D230; Sigma-Aldrich) spin cast on a planar substrate. A lithographically patterned metal layer serves as a hard mask for oxygen plasma etching of the SMP. Transfer of such a 2D SMP structure involves removal of an underlying sacrificial layer and retrieval onto the surface of a water-soluble tape (polyvinyl alcohol; 3M Co.). A thin layer of Ti (5 nm) and SiO_2 (50 nm) deposited at certain locations on the SMP by use of a flexible shadow mask (75 μm thick film of polyimide) define locations (bonding sites; red parts in Figure 1a) that yield surface hydroxyl termination after exposure to ozone. Transfer onto a prestrained silicone elastomer substrate (Dragon Skin; Smooth-On, Easton, PA), also functionalized with surface hydroxyl groups by blanket exposure to ozone, leads to strong, spatially selective bonding due to covalent linkages that result from interfacial condensation reactions, only at the locations of the Ti/SiO_2. At all other locations, comparatively weak van der Waals forces dominate the interfacial interactions. Releasing the prestrain in the elastomer allows it to return to its original shape, thereby inducing large compressive forces on the 2D SMP structure at the bonding sites and formation of a corresponding 3D architecture by mechanical buckling. Macroscale 3D structures described here rely on a 3D printer (Object 260VS, Stratasys) to generate 2D patterns of a UV-curable SMP ink (Veroblue, Stratasys) with thicknesses of 100 μm. The processes for 2D to 3D geometrical transformation are the same as those described above.

Dr. Y. Zhang
Department of Biomedical
Biological and Chemical Engineering
University of Missouri–Columbia
Columbia, MO 65211, USA

Dr. Z. Xie, H. Luan
Departments of Civil and Environmental Engineering
Mechanical Engineering, and Materials Science and Engineering
Northwestern University
Evanston, IL 60208, USA

K. Nan, X. Shan, Z. Wang
Department of Materials Science and Engineering
Frederick Seitz Materials Research Laboratory
University of Illinois at Urbana-Champaign
Urbana, IL 61801, USA

R. Sun
Bristol Composites Institute (ACCIS)
University of Bristol
Bristol BS8 1TR, UK

Z. Xu
The State Key Laboratory for Manufacturing and Systems Engineering
School of Mechanical Engineering
Xi'an Jiaotong University
Xi'an 710049, P. R. China

Prof. Y. Huang
Departments of Civil and Environmental Engineering
Mechanical Engineering, and Materials Science and Engineering
Center for Bio-Integrated Electronics
Northwestern University
Evanston, IL 60208, USA

Prof. J. A. Rogers
Department of Materials Science and Engineering
Biomedical Engineering, Neurological Surgery, Chemistry, Mechanical Engineering, Electrical Engineering and Computer Science
Northwestern University
Evanston, IL 60208, USA

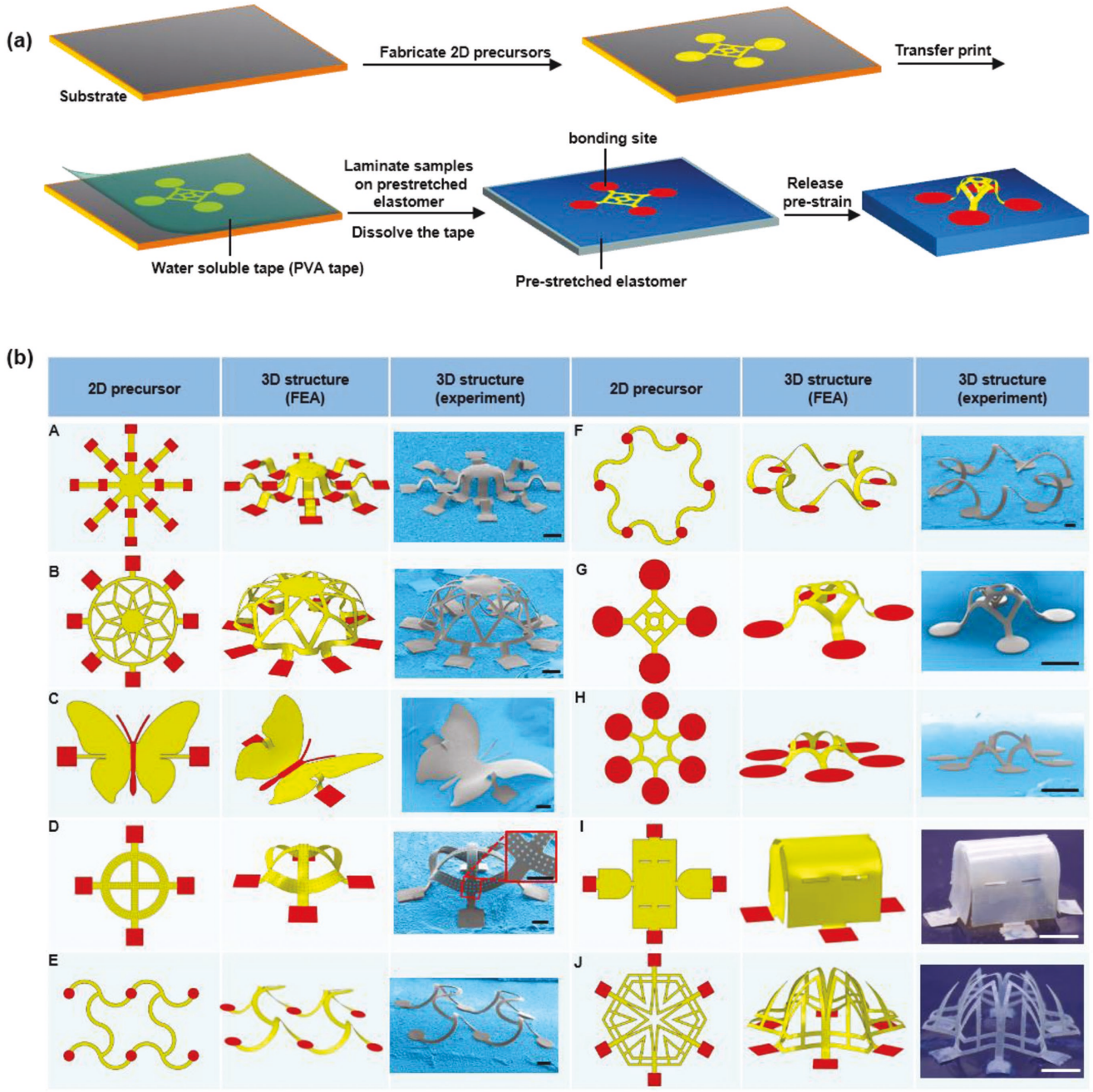

Figure 1. 3D shape memory polymer (SMP) mesostructures formed by mechanically guided assembly. a) Schematic illustration of the fabrication process for 3D SMP mesostructures via photolithography and compressive buckling. b) Experimental (SEM/optical) images and corresponding results of finite-element analysis for various 3D SMP mesostructures. Scale bars, 200 μm for structures A–H, and 5 mm for structures I and J.

Figure 1b presents a collection of experimental results and predictions using 3D finite-element analysis (FEA) for various cases (10 μm thick for structures A–F, 5 μm thick for structures G and H, and 100 μm thick for structures I and J). A rich range of 3D configurations are possible, including those illustrated here that resemble an octopus, butterfly, stadium, treasure box, closed-loop circular helix, and double floor helix. The thicknesses, critical feature sizes, and overall dimensions are as small as 5, 10, 500 μm, but they are extendable to even smaller length scales that lie outside of the limits of many alternative methods in 3D microfabrication of SMP structures.[54,55] An important point is that the steps for preparing the 2D precursors are fully compatible with the most advanced techniques in 2D micro/nanofabrication. A consequence, for example, is the ability to include nano/microscale patterns into the 3D SMP mesostructures. Structure D in Figure 1b shows an array of holes (≈10 μm in depth and ≈10 μm in diameter) distributed across the area of a 2D precursor, yielding a "holey" 3D architecture after assembly. Furthermore, introducing patterns of cuts into the 2D precursors yields 3D SMP structures that

incorporate ideas in kirigami (structure I). In all cases, quantitative mechanics modeling by FEA (see the Experimental Section for details) precisely captures the deformations of the 2D-to-3D transformation process, as evidenced by good agreement with experimental results (Figure 1b). As described subsequently, the SMP materials can serve as supports for functional materials and even fully formed device components, as routes to 3D integrated systems.

SMPs can actively change from their original (permanent) shape to a deformed (temporary) shape by mechanical loading and subsequent fixation of the resulting deformation.[56,57] Exposure to external stimuli, such as heat,[58,59] light,[60] and pH,[61] leads to recovery of the original shapes. The microscale mechanism of this shape fixity and recovery relates to a system of netpoints consisting of physical or chemical bonds, and connecting chain segments that switch their flexibility and mobility upon exposure to external stimuli (e.g., heat) as mentioned above. In a typical shape memory cycle, heating above the glass temperature of the chain segments (T_{trans}) enables their high flexibility and mobility (Figure S1, Supporting Information), which is followed by deformation via an external force. Cooling to below T_{trans} "locks" the chains in place in a high-energy state. When the temperature increases above T_{trans}, the chains regain mobility and return to their original maximum entropy state, corresponding to the relaxed macroscopic shape. In this work, the glass transition temperatures are ≈57 and ≈64 °C for SMP films used in the micro- and macroscale 3D architectures, respectively, as shown by the results of dynamic mechanical analysis (DMA) testing in Figure S2 in the Supporting Information. Below T_{trans}, e.g., at room temperature (25 °C) SMP has a storage modulus of ≈3 GPa, on the same order of those of commonly used polymers, such as polyimide and SU8. Above T_{trans}, SMP becomes very soft and highly stretchable, with a storage modulus of ≈10 MPa. In this work, the shape fixity of SMPs serves as a technique for the realization of freestanding 3D architectures and electronics, as well as other capabilities described subsequently.

Figure 2 demonstrates that the shape fixing effect of SMPs allows access to fully freestanding 3D mesostructures. As schematically shown in Figure 2a, a full cycle of heating and cooling across T_{trans} fixes the assembled 3D SMP shapes such that release from the assembly platform by eliminating an underlying sacrificial layer releases the structure without altering its 3D shape. Specifically, the heating and cooling occur in an oven set to 70 °C for 1 min and under ambient conditions (25 °C), respectively. The sacrificial layer consists of a film of magnesium (Mg, 200 nm in thickness) formed at the bonding sites in the 2D precursor stage of the process, and removed by immersion in water in the 3D mesostructured stage. Figure 2b and Figure S3 in the Supporting Information show various freestanding 3D SMP structures (10 μm in thickness for structures A–C, E, and F, and 100 μm in thickness for structures D, G, and H), each held at one of the bonding sites by an atomic force microscope (AFM) tip. Illustrative examples include flowers, baskets, and others. Due to the freezing of SMP chain segments at the microscale, these freestanding mesostructures maintain their 3D configurations, as qualitatively studied and quantitatively characterized in this work. A comparison of the optical images of 3D SMP structures on a substrate and in a freestanding state (structures E–H in Figure 2b) demonstrates that there is no obvious shape recovery of 3D SMP architectures after the release from the assembly platform. To quantify the shape recovery, the overall lateral dimensions of the 3D structure, i.e., the distance between two bonding sites with the largest lateral separation, before and after the release from the substrate are defined as L_0 and L_1, respectively, as schematically shown in Figure 2a. L_0 and L_1 are 1.733 and 1.727 mm, respectively, for structure E in Figure 2b. Table S1 (Supporting Information) shows measured and calculated L_0 and L_1 for three additional structures F, G, and H. Here, a multibranch viscoelastic model is adopted to capture the shape fixing and recovery properties of SMP, whose parameters are fitted by the DMA test (Figure S2, and Tables S2 and S3, Supporting Information). To quantify the shape fixation of a freestanding 3D SMP architecture, the shape storage ratio is defined as follows

$$\varepsilon_s = 1 - \frac{|L_1 - L_0|}{L_0} \times 100\%$$

The shape storage ratios are determined to be 99.65%, 100%, 98.85%, and 98.69% for structures E, F, G, and H, which agree reasonably well with the calculated results (99.56%, 99.17%, 98.6%, and 99.12%, respectively). Such small/no change in the lateral size of the 3D structure before and after the release from the substrate highlights the fidelity of the process. The parallelism of the overall approach allows fabrication of many freestanding structures from a single assembly platform in a single set of processing steps, as shown in Figure 2d.

Integrating functional materials and components onto the 2D SMP precursors provides immediate access to freestanding 3D functional devices, as shown for the case of wirelessly powered light emitting systems in **Figure 3**. The fabrication begins with spin-coating films of SMPs (20 μm in thickness) on copper foils (18 μm in thickness), followed by photolithographic patterning and wet etching of the copper to define coil antennas and interconnects for light-emitting diodes (LEDs) and capacitors (Figure 3a). Laser cutting defines patterns in the SMP film, as the supporting and shape fixing layer. Formation of freestanding 3D architectures from these 2D functional precursors follows the 3D buckling and shape fixation schemes introduced earlier. Positioning these devices inside an external loop antenna with applied radio frequency power at a frequency of 13.56 MHz leads to power transfer to activate the LEDs. Figure 3b shows the inductance and Q factor obtained by electromagnetic simulation for the coil, which has a diameter of 7 mm. A capacitor of 39 pF enables impedance matching at 13.56 MHz. The relative high Q factor (≈27 at 13.56 MHz) ensures high efficiency in power transfer. The scattering parameter S11 (≈22 dB) shown in Figure 3c indicates a low return loss in this system. Figure 3d provides some experimental demonstrations. Devices A (7 mm diameter antenna) and B–D (8 mm diameter antennas; Figure S4, Supporting Information) in Figure 3d include single and multiple LEDs. These simple examples suggest a broad range of possibilities in other types of electronic and optoelectronic devices. Furthermore, we have qualitatively and quantitatively investigated the mechanical stability of the fabricated freestanding electronics and structures (Figure 3e; Figure S5 and Videos S1–S5, Supporting Information). Three freestanding 3D structures and one freestanding

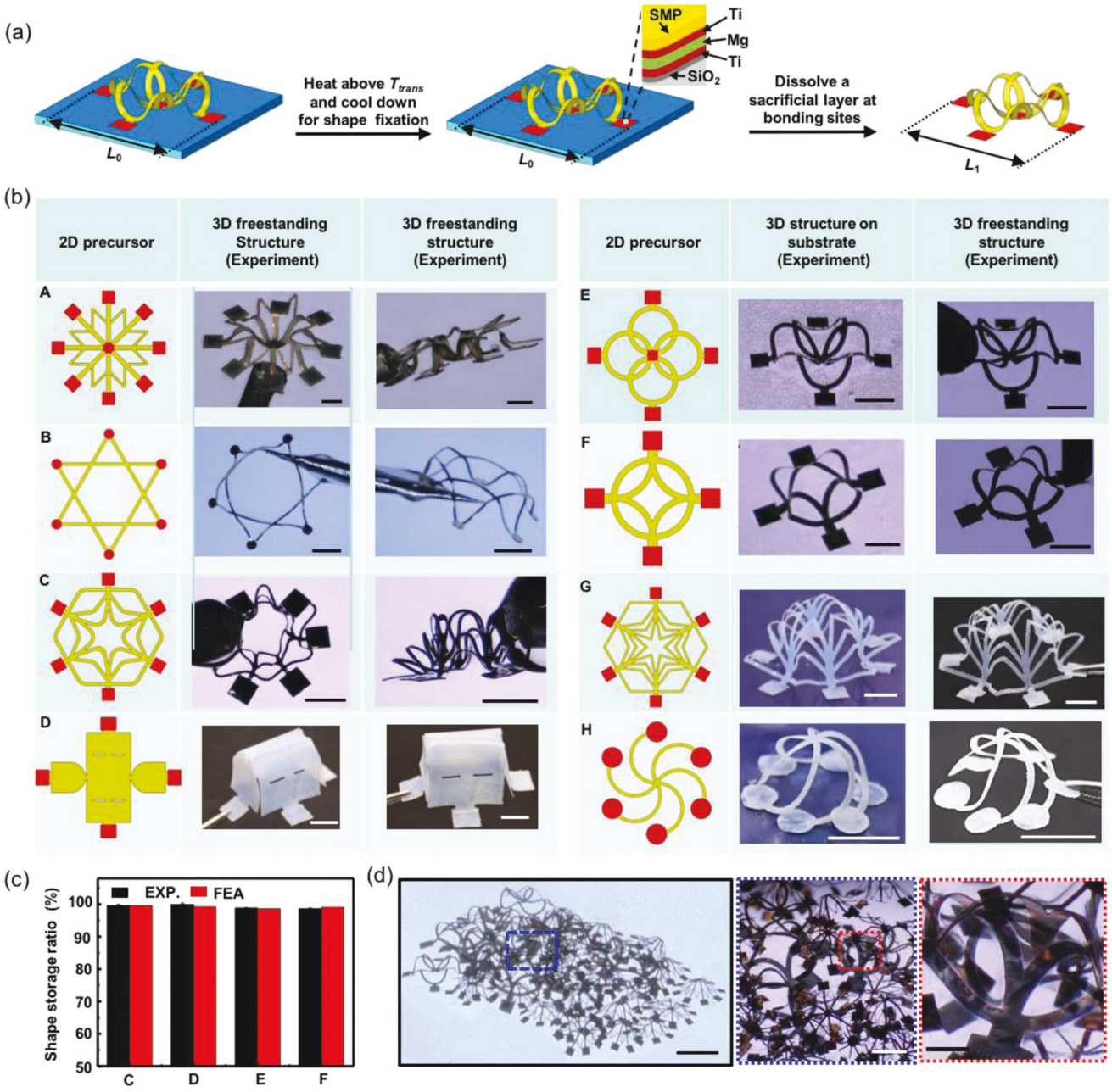

Figure 2. Freestanding 3D mesostructures enabled by the shape fixity characteristics of SMPs. a) Schematic illustration of the fabrication process of freestanding 3D SMP mesostructures. b) Optical images and FEA results of various freestanding 3D mesostructures. Scale bars, 500 μm for structures A–C and E–F, and 5 mm for structures D, G, and H. c) Experimental and FEA results of the shape storage ratios for four different 3D mesostructures. d) Optical images of piled freestanding 3D mesostructures. Scale bars, 1 mm, 500 μm, and 200 μm from left to right.

3D electronic device are deformed along the out-of-plane direction, using a tweezer under room temperature. After removing the external force, the 3D structure and electronic device recover their original shapes without any noticeable damage, indicating a level of mechanical robustness that might be necessary for many applications. The thermal effect from the operation of 3D electronics can be evaluated by monitoring the temperature and shape change under operation conditions. Results show that the device maintains a nearly constant temperature for an operation period of 2 h without any shape change (Figure 3f; Figure S6, Supporting Information). The techniques reported here can be applied to other SMPs with a broad range of T_{trans}, suggesting a wide scope of potential applications,[62–66] including those that require operation at elevated temperatures.

In addition to freestanding 3D architectures and electronic devices, another important attribute that follows from the use of SMPs is in shape recovery. **Figure 4**a and Figure S7 in the Supporting Information show experimental and FEA results for a complete shape memory cycle for three different 3D SMP architectures. While heated to temperatures above T_{trans} (57 °C)

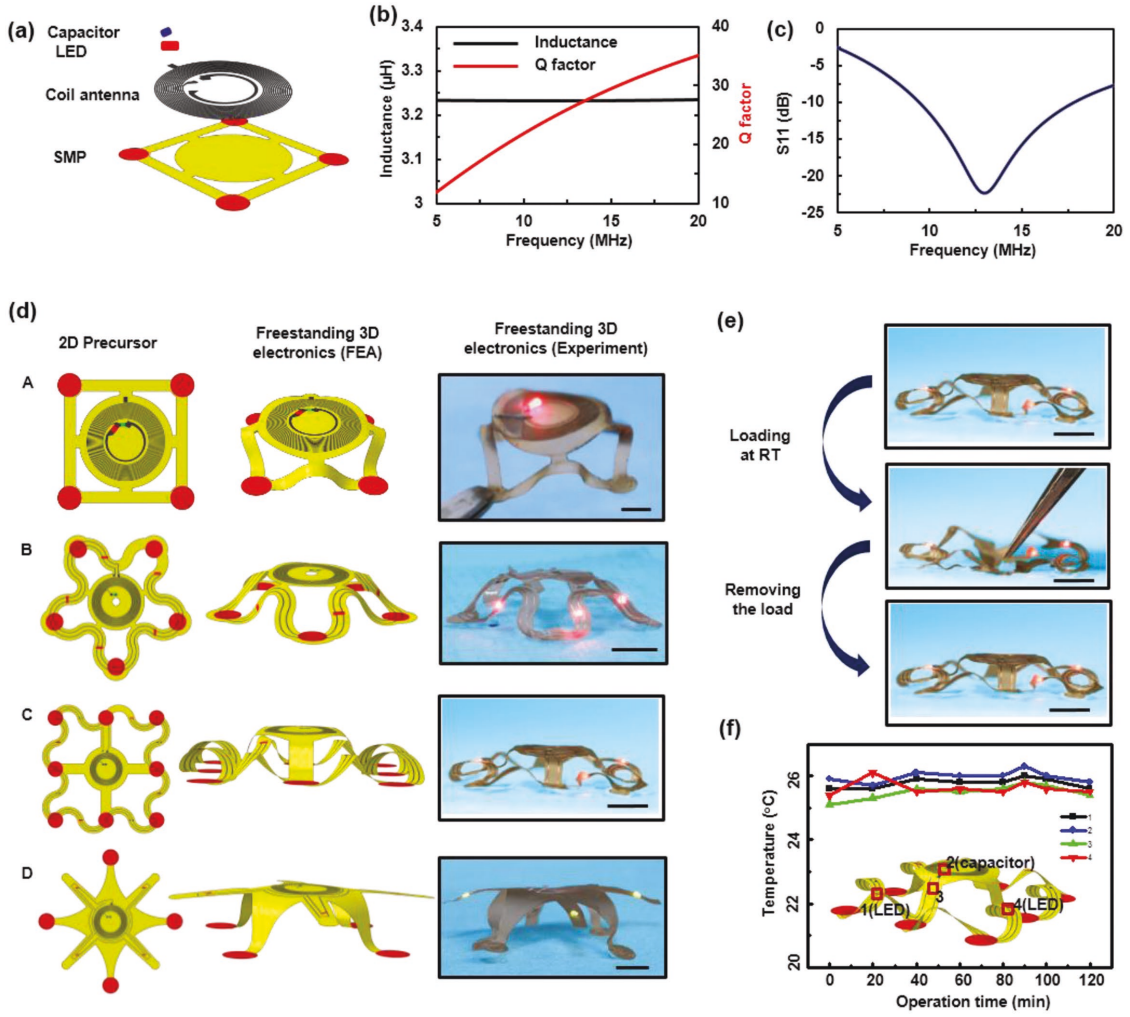

Figure 3. Freestanding 3D electronics. a) Schematic illustration of the multilayer 2D precursor in an explosive view, including the SMP support, coil antenna, capacitor, and LEDs. b,c) Computational modeling of the inductance, *Q* factor, and S11 characteristics of the coil antenna. d) Freestanding 3D electronics with microscale LEDs, capacitor, and coil antenna integrated with SMP structures. When the freestanding 3D structures are positioned inside an external loop antenna, LEDs are turned on due to near field communication (NFC) between the coil antenna and the external loop antenna. Scale bars, 2 mm. e) Optical images showing freestanding 3D electronic device before deformation, being deformed and after load removal. Scale bars, 2 mm. f) Temperature curves of four representative locations at a freestanding electronic device as a function of operation time.

with a soldering gun, localized forces delivered with a three-axis stage (Thorlabs, Inc., Newton, NJ) deform the 3D structure into two different temporary shapes (mode I and mode II). Cooling to room temperature while maintaining the applied force fixes the temporary shapes. Figure 4a shows complete shape recovery by heating the deformed 3D SMP structures to temperatures above 57 °C for a few seconds. The rapid speed and the fidelity of the recovery process are consistent with a well-behaved shape memory effect in these materials. A viscoelastic model based on FEA enables quantitative modeling of the entire process. The color in the FEA results (Figure 4a) denotes the distribution of maximum principal strains in the SMPs. The peak strain values during deformations under $T > T_{trans}$ remain well below the corresponding fracture thresholds (a few hundreds of percent) of the SMP,[66] thereby ensuring structural integrity. In addition, we have qualitatively and quantitatively investigated the reproducibility of shape recovery in thermal cycles (Figure S8, Supporting Information). The results show that the shape recovery of the fabricated 3D structures is highly reproducible after a number of thermal cycles. The shape reprogrammable feature can expand the range of accessible 3D geometries beyond those possible by compressive buckling directly via controlled mechanical loading.

In addition to control of the ambient environment, illuminating an absorbing SMP with light can induce the necessary increases in temperature.[67] Optical absorption can be enhanced by the addition of conductive fillers, such as ceramics, carbon black, and nanoparticles.[68–70] Results presented here use coatings of gold (Au) nanoparticles with plasmonic absorption resonances in the near-infrared region of the visible spectrum (808 nm, Nanopartz Inc., Loveland, CO, USA) applied to the 2D SMP precursors (Figure S9, Supporting Information; Figure 4b).[47] Deformation of the resulting 3D architectures occurs via forces applied with a three-axis stage at a temperature

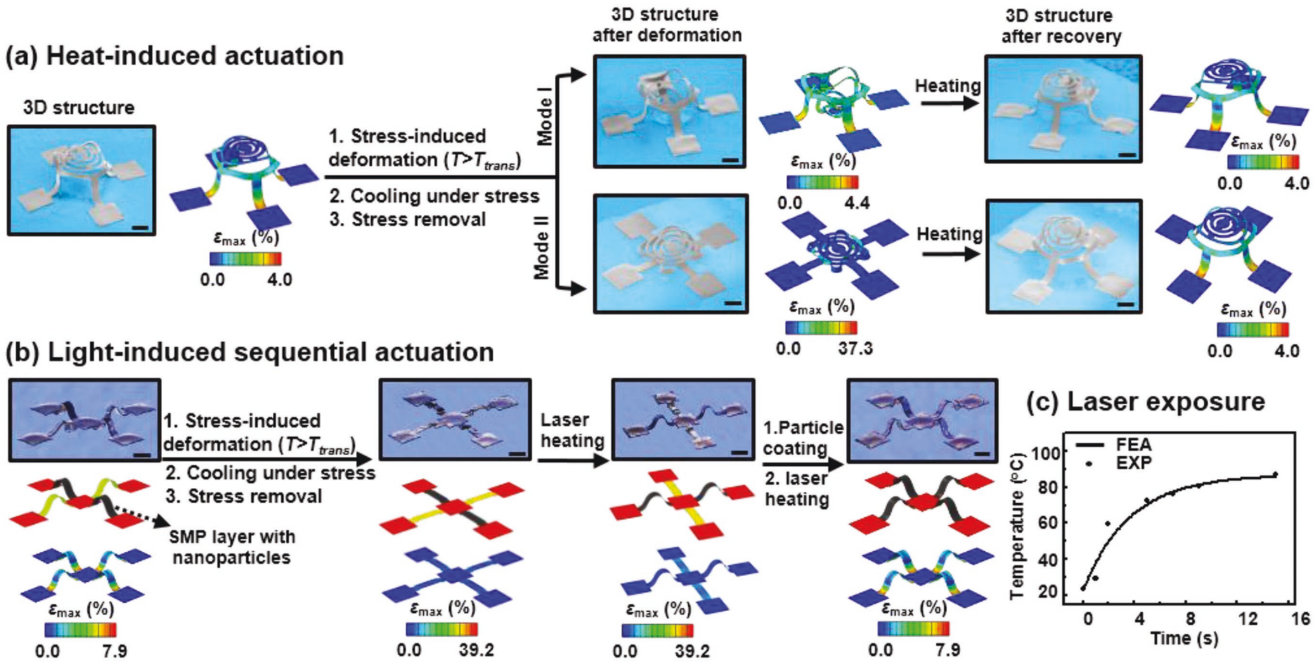

Figure 4. Actuation of 3D SMP mesostructures. a) SEM images and FEA results on a shape memory cycle of a 3D SMP mesostructure. Scale bars, 400 µm. b) Optical images, FEA results, and schematic illustration on the sequential actuation of a 3D SMP mesostructure via selectively coating gold nanoparticles on the 3D structure followed by laser heating. Scale bars, 1 mm. c) Experimental and FEA results of the temperature of nanoparticle-coated SMPs as a function of laser exposure time.

above T_{trans}. The deformed 3D architecture recovers its original shape after exposure to a laser (808 nm, 300 mW, Biglasers company, Monroe, NY) for a few seconds. An additional capability associated with this approach follows from coating the nanoparticles selectively on different parts of a 3D mesostructure (Figure 4b) or selectively illuminating certain regions for sequential shape recovery. Figure 4c shows the temperature of this structure measured with an infrared camera as a function of laser exposure time. Due to the ultrathin geometry, the temperature is, to a good approximation, uniform through the thickness (Figure S10, Supporting Information). The temperature of the SMP film (15 µm) increases from room temperature (25 °C) to T_{trans} (57 °C) after exposure to laser light for only two to three seconds. Under light illumination, the deformed 3D structure recovers its original shape quickly (Figure S11, Supporting Information). Here, the experimentally measured temperature as a function of time serves as an input for computational modeling. The results allow for shapes that include the combined effects of 3D assembly and local deformation/recovery. The additional design versatility has important applications in actuators, microrobotics, and minimally invasive biomedical devices.

As described here, combining the shape fixation characteristics of SMP with mechanically guided approaches to 3D structure formation yields an attractive scheme to manufacturing of freestanding 3D architectures and functional devices across length scales from micrometers to centimeters. Demonstrations include a diversity of freestanding 3D mesostructures, such as those that resemble the flower, basket, and helix. The integration of electronic components to SMPs provides access to freestanding 3D functional devices, as demonstrated in wirelessly powered LEDs integrated with 3D architectures. Shape recovery and shape programmability represent two additional capabilities that follow from this same overall scheme. These results create unusual routes to freestanding 3D mesostructures and programmable microdevices for potential applications that cannot be addressed using other approaches. Furthermore, the technique applies to other SMP materials with a broad range of glass transition temperatures for a wide scope of applications.

Experimental Section

SMP Synthesis and 3D SMP Structure Assembly: Epoxy monomer E44 (molecular weight ≈450 g mol^{-1}) and curing agent poly(propylene glycol) bis(2-aminopropyl)ether (Jeffamine D230), purchased from China Petrochemical Corporation and Sigma-Aldrich, respectively, were used as received without purification. Preparation of 3D SMP structures began with the spin coating of a thin sacrificial layer of water-soluble polymer (poly(4-styrenesulfonic acid), Sigma-Aldrich) onto a silicon wafer, followed by spin coating a mixture of E44 and D230 with a mass ratio of 44:23. The intrinsic material properties of SMPs, including their mechanical characteristics, can be adjusted by selection of molecular parameters, such as the type of monomer or the comonomer ratio. Curing the SMP samples occurred at 110 °C in a furnace for 1 h. A thin layer of chromium (Cr, 10 nm) and gold (Au, 50 nm) deposited on the SMP by electron beam evaporation and patterned by photolithography and wet etching served as a hard mask for oxygen plasma etching of the SMP. Immersion in water partially dissolved the underlying water-soluble layer, thereby releasing the entire structure from the silicon wafer. A soft silicone elastomer substrate (Dragon Skin; Smooth-On, Easton, PA) stretched and then exposed to ozone served as an assembly platform. Transfer printing of the 2D precursor after selective deposition of a thin layer of Ti (5 nm) and SiO_2 (50 nm) onto targeted sites of its back surface led to strong adhesion only at the bonding sites. Allowing the substrate to return to its original shape led to buckling and geometry transformation

to the targeted 3D shape. The preparation of macroscale 3D architectures began with the fabrication of 2D precursors in Veroblue with a 3D printer (Object 260VS, Stratasys) into desired patterns, followed by transfer onto a prestretched silicone substrate (2 mm in thickness, Dragon Skin, Smooth-On). A commercial adhesive (Super Glue, Gorilla Glue Company) yielded strong mechanical bonds at desired locations after curing at room temperature for several minutes. Slowly releasing the prestretched elastomer substrate initiated the 3D assembly process.

Actuation of 3D SMP Structures: Thermally induced actuation relied on heating to ≈70 °C with a soldering gun and then applying forces at this temperature with a three-axis stage (Thorlabs Inc.). Maintaining these forces during cooling to room temperature retained the deformed shapes. Recovery to the original shapes followed from heating due to the shape memory effect. Light-induced actuation used 2D patterns of SMP films (20 μm thick) coated with Au nanoparticles (808 nm wavelength for resonant absorption, Nanopartz Inc.). After the deformation as previously discussed, exposure to infrared laser light (808 nm, 300 mW, Biglasers company) led to shape recovery.

Freestanding 3D SMPs: A thin layer of magnesium (Mg; 200 nm) deposited by electron beam evaporation served as a sacrificial layer between the SMP and Ti/SiO_2 layer at the bonding sites. After formation, 3D structures attached to the elastomer substrate were heated to 70 °C for 1 min in an oven. Cooling to room temperature fixed the 3D shape such that immersion in water dissolved the Mg layer and released freestanding 3D structures.

Freestanding 3D Electronics: The fabrication of freestanding 3D electronic systems began with spin-coating films of SMPs onto 18 μm thick Cu foils. Spin casting and photolithographic patterning of a photoresist (AZ5214, 1.6 μm in thickness) yielded a mask for wet etching (CE-100 etchant, Transene, etchant rate ≈1 μm min^{-1}) of the copper foil to define Cu traces for coil antennas and interconnects to electronic components. Laser cutting defined patterns in the SMPs. Placing LEDs and capacitors at selectively defined locations on the 2D patterns with conductive epoxy (Allied Electronics Corp., Fort Worth, TX) completed the integration of electronics with SMPs in the 2D format. The integrated SMP/electronics were assembled into 3D architectures with the mechanics-guided assembly technique previously introduced. The shape fixing effect of SMPs allowed access to freestanding 3D electronics.

Finite-Element Analysis: Simulations of the postbuckling processes used finite-element analysis software (ABAQUS) to determine the final 3D configurations through mechanically guided assembly. Eight-node 3D solid elements (C3D8R) and four-node shell elements (S4R) were used for the silicone substrate and 2D precursors, respectively. Refined meshes were adopted to ensure the accuracy. The elastic modulus (E) and Poisson's ratio (υ) are $E_{substrate}$ = 166 kPa and $\upsilon_{substrate}$ = 0.49 for the substrate, and E_{Cu} = 119 GPa and υ_{Cu} = 0.34 for copper (Cu). For the SMP used in this study, a multibranch viscoelastic model[54,71] captured the thermo-viscoelastic and shape memory behaviors, with parameters provided in Tables S2 and S3 (Supporting Information).

Electromagnetic Simulations: Electromagnetic simulations based on the finite-element method defined the inductance, Q factor, and scattering parameter S11 (for 8 mm and 7 mm diameter loop antennas matching with 47 and 39 pF capacitors, respectively) of the RF system. The simulations were performed using the commercial software ANSYS HFSS, where the lumped port was used to obtain the scattering parameter S11 and port impendence Z. The LEDs (with 400 Ω resistance) were modeled through the lumped RLC boundaries in the numerical simulations. The adaptive mesh (tetrahedron elements) was adopted to ensure computational accuracy. The inductance (L) and Q factor (Q) (as shown in Figure 4 and Figure S4 in the Supporting Information) were obtained from the real and imaginary parts of the Z, and the working frequency, respectively.

Supporting Information

Supporting Information is available from the Wiley Online Library or from the author.

Acknowledgements

X.W., X.G., and J.Y. contributed equally to this work. The authors acknowledge the support from the U.S. Department of Energy, Office of Science, Basic Energy Sciences (Grant No. DE-FG02-07ER46471). Y.Z. acknowledges the support from the National Natural Science Foundation of China (Grant Nos. 11502129 and 11722217) and the Tsinghua National Laboratory for Information Science and Technology. Y.H. acknowledges the support from the NSF (Grant Nos. CMMI1400169, CMMI1534120, and CMMI1635443). R.S. acknowledges support from the Engineering and Physical Sciences Research Council (Grant No. EP/ L016028/1). X.G. acknowledges support from the National Natural Science Foundation of China (Grant No. 11702155). Z.X. acknowledges the support National Natural Science Foundation of China (Grant No. 11402134).

Conflict of Interest

The authors declare no conflict of interest.

Keywords

3D microstructures, 3D printing, 4D printing, guided assembly, shape memory polymers

Received: August 29, 2018
Revised: October 2, 2018
Published online: October 29, 2018

[1] M. S. Mannoor, Z. Jiang, T. James, Y. L. Kong, K. A. Malatesta, W. O. Soboyejo, N. Verma, D. H. Gracias, M. C. McAlpine, *Nano Lett.* **2013**, *13*, 2634.
[2] T. G. Leong, C. L. Randall, B. R. Benson, N. Bassik, G. M. Stern, D. H. Gracias, *Proc. Natl. Acad. Sci. USA* **2009**, *106*, 703.
[3] R. Feiner, L. Engel, S. Fleischer, M. Malki, I. Gal, A. Shapira, Y. Shacham-Diamand, T. Dvir, *Nat. Mater.* **2016**, *15*, 679.
[4] X. Liu, H. Yuk, S. Lin, G. A. Parada, T. C. Tang, E. Tham, C. de la Fuente-Nunez, T. K. Lu, X. Zhao, *Adv. Mater.* **2018**, *30*, 1704821.
[5] B. Z. Tian, J. Liu, T. Dvir, L. H. Jin, J. H. Tsui, Q. Qing, Z. G. Suo, R. Langer, D. S. Kohane, C. M. Lieber, *Nat. Mater.* **2012**, *11*, 986.
[6] J. Valentine, S. Zhang, T. Zentgraf, E. Ulin-Avila, D. A. Genov, G. Bartal, X. Zhang, *Nature* **2008**, *455*, 376.
[7] T. A. Schaedler, A. J. Jacobsen, A. Torrents, A. E. Sorensen, J. Lian, J. R. Greer, L. Valdevit, W. B. Carter, *Science* **2011**, *334*, 962.
[8] C. M. Soukoulis, M. Wegener, *Nat. Photonics* **2011**, *5*, 523.
[9] X. Zheng, H. Lee, T. H. Weisgraber, M. Shusteff, J. DeOtte, E. B. Duoss, J. D. Kuntz, M. M. Biener, Q. Ge, J. A. Jackson, S. O. Kucheyev, N. X. Fang, C. M. Spadaccini, *Science* **2014**, *344*, 1373.
[10] Y. C. Tang, G. J. Lin, S. Yang, Y. K. Yi, R. D. Kamien, J. Yin, *Adv. Mater.* **2017**, *29*, 1604262.
[11] W. Liu, Z. Chen, G. M. Zhou, Y. M. Sun, H. R. Lee, C. Liu, H. B. Yao, Z. N. Bao, Y. Cui, *Adv. Mater.* **2016**, *28*, 3578.
[12] H. Zhang, X. Yu, P. V. Braun, *Nat. Nanotechnol.* **2011**, *6*, 277.
[13] J. H. Pikul, H. Gang Zhang, J. Cho, P. V. Braun, W. P. King, *Nat. Commun.* **2013**, *4*, 1732.
[14] T. S. Wei, B. Y. Ahn, J. Grotto, J. A. Lewis, *Adv. Mater.* **2018**, *30*, 1703027.
[15] K. Dong, J. Deng, Y. Zi, Y. C. Wang, C. Xu, H. Zou, W. Ding, Y. Dai, B. Gu, B. Sun, Z. L. Wang, *Adv. Mater.* **2017**, *29*, 1702648.
[16] Z. Song, T. Ma, R. Tang, Q. Cheng, X. Wang, D. Krishnaraju, R. Panat, C. K. Chan, H. Yu, H. Jiang, *Nat. Commun.* **2014**, *5*, 3140.

[17] B. Y. Ahn, E. B. Duoss, M. J. Motala, X. Y. Guo, S. I. Park, Y. J. Xiong, J. Yoon, R. G. Nuzzo, J. A. Rogers, J. A. Lewis, *Science* **2009**, *323*, 1590.
[18] D. Grimm, C. C. Bof Bufon, C. Deneke, P. Atkinson, D. J. Thurmer, F. Schaffel, S. Gorantla, A. Bachmatiuk, O. G. Schmidt, *Nano Lett.* **2013**, *13*, 213.
[19] K. Zhang, Y. H. Jung, S. Mikael, J. H. Seo, M. Kim, H. Mi, H. Zhou, Z. Xia, W. Zhou, S. Gong, Z. Ma, *Nat. Commun.* **2017**, *8*, 1782.
[20] K. I. Jang, K. Li, H. U. Chung, S. Xu, H. N. Jung, Y. Yang, J. W. Kwak, H. H. Jung, J. Song, C. Yang, A. Wang, Z. Liu, J. Y. Lee, B. H. Kim, J. H. Kim, J. Lee, Y. Yu, B. J. Kim, H. Jang, K. J. Yu, J. Kim, J. W. Lee, J. W. Jeong, Y. M. Song, Y. Huang, Y. Zhang, J. A. Rogers, *Nat. Commun.* **2017**, *8*, 15894.
[21] Z. G. Zheng, C. L. Yuan, W. Hu, H. K. Bisoyi, M. J. Tang, Z. Liu, P. Z. Sun, W. Q. Yang, X. Q. Wang, D. Shen, Y. Li, F. Ye, Y. Q. Lu, G. Li, Q. Li, *Adv. Mater.* **2017**, *29*, 1703165.
[22] S. Z. Guo, K. Qiu, F. Meng, S. H. Park, M. C. McAlpine, *Adv. Mater.* **2017**, *29*, 1701218.
[23] Z. Liu, D. Qi, W. R. Leow, J. Yu, M. Xiloyannnis, L. Cappello, Y. Liu, B. Zhu, Y. Jiang, G. Chen, L. Masia, B. Liedberg, X. Chen, *Adv. Mater.30*, **2018**, 1707285.
[24] H. Yang, W. R. Leow, T. Wang, J. Wang, J. Yu, K. He, D. Qi, C. Wan, X. Chen, *Adv. Mater.* **2017**, *29*, 1701627.
[25] C. Yuan, D. J. Roach, C. K. Dunn, Q. Mu, X. Kuang, C. M. Yakacki, T. J. Wang, K. Yu, H. J. Qi, *Soft Matter* **2017**, *13*, 5558.
[26] B. G. Compton, J. A. Lewis, *Adv. Mater.* **2014**, *26*, 5930.
[27] D. B. Kolesky, R. L. Truby, A. S. Gladman, T. A. Busbee, K. A. Homan, J. A. Lewis, *Adv. Mater.* **2014**, *26*, 3124.
[28] W. Zhu, J. Li, Y. J. Leong, I. Rozen, X. Qu, R. Dong, Z. Wu, W. Gao, P. H. Chung, J. Wang, S. Chen, *Adv. Mater.* **2015**, *27*, 4411.
[29] A. Cangialosi, C. Yoon, J. Liu, Q. Huang, J. Guo, T. D. Nguyen, D. H. Gracias, R. Schulman, *Science* **2017**, *357*, 1126.
[30] B. Zhang, K. Kowsari, A. Serjouei, M. L. Dunn, Q. Ge, *Nat. Commun.* **2018**, *9*, 1831.
[31] R. L. Truby, M. Wehner, A. K. Grosskopf, D. M. Vogt, S. G. M. Uzel, R. J. Wood, J. A. Lewis, *Adv. Mater.* **2018**, *30*, 1706383.
[32] L. C. Hsiao, A. Z. Badruddoza, L. C. Cheng, P. S. Doyle, *Soft Matter* **2017**, *13*, 921.
[33] S. Y. Lin, J. G. Fleming, D. L. Hetherington, B. K. Smith, R. Biswas, K. M. Ho, M. M. Sigalas, W. Zubrzycki, S. R. Kurtz, J. Bur, *Nature* **1998**, *394*, 251.
[34] S. Noda, K. Tomoda, N. Yamamoto, A. Chutinan, *Science* **2000**, *289*, 604.
[35] M. Qi, E. Lidorikis, P. T. Rakich, S. G. Johnson, J. D. Joannopoulos, E. P. Ippen, H. I. Smith, *Nature* **2004**, *429*, 538.
[36] Z. Yan, M. Han, Y. Shi, A. Badea, Y. Yang, A. Kulkarni, E. Hanson, M. E. Kandel, X. Wen, F. Zhang, Y. Luo, Q. Lin, H. Zhang, X. Guo, Y. Huang, K. Nan, S. Jia, A. W. Oraham, M. B. Mevis, J. Lim, X. Guo, M. Gao, W. Ryu, K. J. Yu, B. G. Nicolau, A. Petronico, S. S. Rubakhin, J. Lou, P. M. Ajayan, K. Thornton, G. Popescu, D. Fang, J. V. Sweedler, P. V. Braun, H. Zhang, R. G. Nuzzo, Y. Huang, Y. Zhang, J. A. Rogers, *Proc. Natl. Acad. Sci. USA* **2017**, *114*, E9455.
[37] C. Py, P. Reverdy, L. Doppler, J. Bico, B. Roman, C. N. Baroud, *Phys. Rev. Lett.* **2007**, *98*, 156103.
[38] Y. Yang, E. M. Terentjev, Y. Wei, Y. Ji, *Nat. Commun.* **2018**, *9*, 1906.
[39] E. Hawkes, B. An, N. M. Benbernou, H. Tanaka, S. Kim, E. D. Demaine, D. Rus, R. J. Wood, *Proc. Natl. Acad. Sci. USA* **2010**, *107*, 12441.
[40] Y. Mao, Y. Zheng, C. Li, L. Guo, Y. Pan, R. Zhu, J. Xu, W. Zhang, W. Wu, *Adv. Mater.* **2017**, *29*, 1606482.
[41] W. A. Xu, Z. Qin, C. T. Chen, H. R. Kwag, Q. L. Ma, A. Sarkar, M. J. Buehler, D. H. Gracias, *Sci. Adv.* **2017**, *3*, e1701084.
[42] Y. Xia, G. Cedillo-Servin, R. D. Kamien, S. Yang, *Adv. Mater.* **2016**, *28*, 9637.
[43] S. Yang, I. S. Choi, R. D. Kamien, *MRS Bull.* **2016**, *41*, 130.
[44] Y. H. Zhang, F. Zhang, Z. Yan, Q. Ma, X. L. Li, Y. G. Huang, J. A. Rogers, *Nat. Rev. Mater.* **2017**, *2*, 17019.
[45] M. J. Liu, G. S. Huang, P. Feng, Q. L. Guo, F. Shao, Z. Tian, G. J. Li, Q. Wan, Y. F. Mei, *J. Semicond.* **2017**, *38*, 064006.
[46] H. M. Fahad, H. Shiraki, M. Amani, C. C. Zhang, V. S. Hebbar, W. Gao, H. Ota, M. Hettick, D. Kiriya, Y. Z. Chen, Y. L. Chueh, A. Javey, *Sci. Adv.* **2017**, *3*, e1602557.
[47] S. Xu, Z. Yan, K. I. Jang, W. Huang, H. R. Fu, J. Kim, Z. Wei, M. Flavin, J. McCracken, R. Wang, A. Badea, Y. Liu, D. Q. Xiao, G. Y. Zhou, J. Lee, H. U. Chung, H. Y. Cheng, W. Ren, A. Banks, X. L. Li, U. Paik, R. G. Nuzzo, Y. G. Huang, Y. H. Zhang, J. A. Rogers, *Science* **2015**, *347*, 154.
[48] Y. Zhang, Z. Yan, K. Nan, D. Xiao, Y. Liu, H. Luan, H. Fu, X. Wang, Q. Yang, J. Wang, W. Ren, H. Si, F. Liu, L. Yang, H. Li, J. Wang, X. Guo, H. Luo, L. Wang, Y. Huang, J. A. Rogers, *Proc. Natl. Acad. Sci. USA* **2015**, *112*, 11757.
[49] Z. Yan, F. Zhang, J. Wang, F. Liu, X. Guo, K. Nan, Q. Lin, M. Gao, D. Xiao, Y. Shi, Y. Qiu, H. Luan, J. H. Kim, Y. Wang, H. Luo, M. Han, Y. Huang, Y. Zhang, J. A. Rogers, *Adv. Funct. Mater.* **2016**, *26*, 2629.
[50] K. I. Jang, K. Li, H. U. Chung, S. Xu, H. N. Jung, Y. Y. Yang, J. W. Kwak, H. H. Jung, J. Song, C. Yang, A. Wang, Z. J. Liu, J. Y. Lee, B. H. Kim, J. H. Kim, J. Lee, Y. Yu, B. J. Kim, H. Jang, K. J. Yu, J. Kim, J. W. Lee, J. W. Jeong, Y. M. Song, Y. G. Huang, Y. H. Zhang, J. A. Rogers, *Nat. Commun.* **2017**, *8*, 15894.
[51] H. Fu, K. Nan, W. Bai, W. Huang, K. Bai, L. Lu, C. Zhou, Y. Liu, F. Liu, J. Wang, M. Han, Z. Yan, H. Luan, Y. Zhang, Y. Zhang, J. Zhao, X. Cheng, M. Li, J. W. Lee, Y. Liu, D. Fang, X. Li, Y. Huang, Y. Zhang, J. A. Rogers, *Nat. Mater.* **2018**, *17*, 268.
[52] Y. Shi, F. Zhang, K. W. Nan, X. J. Wang, J. T. Wang, Y. J. Zhang, Y. T. Zhang, H. W. Luan, K. C. Hwang, Y. G. Huang, J. A. Rogers, Y. H. Zhang, *Extreme Mech. Lett.* **2017**, *15*, 151.
[53] Z. Yan, M. D. Han, Y. Shi, A. Badea, Y. Y. Yang, A. Kulkarni, E. Hanson, M. E. Kandel, X. W. Wen, F. Zhang, Y. Y. Luo, Q. Lin, H. Zhang, X. G. Guo, Y. M. Huang, K. W. Nan, S. Jia, A. W. Oraham, M. B. Mevis, J. M. Lim, X. L. Guo, M. Y. Gao, W. Ryu, K. J. Yu, B. G. Nicolau, A. Petronico, S. S. Rubakhin, J. Lou, P. M. Ajayan, K. Thornton, G. Popescu, D. N. Fang, J. V. Sweedler, P. V. Braun, H. X. Zhang, R. G. Nuzzo, Y. G. Huang, Y. H. Zhang, J. A. Rogers, *Proc. Natl. Acad. Sci. USA* **2017**, *114*, E9455.
[54] Z. Ding, C. Yuan, X. R. Peng, T. J. Wang, H. J. Qi, M. L. Dunn, *Sci. Adv.* **2017**, *3*, e1602890.
[55] M. Zarek, M. Layani, I. Cooperstein, E. Sachyani, D. Cohn, S. Magdassi, *Adv. Mater.* **2016**, *28*, 4449.
[56] M. Behl, A. Lendlein, *Mater. Today* **2007**, *10*, 20.
[57] H. Yang, W. R. Leow, T. Wang, J. Wang, J. C. Yu, K. He, D. P. Qi, C. J. Wan, X. D. Chen, *Adv. Mater.* **2017**, *29*, 1701627.
[58] V. Srivastava, S. A. Chester, L. Anand, *J. Mech. Phys. Solids* **2010**, *58*, 1100.
[59] H. Koerner, G. Price, N. A. Pearce, M. Alexander, R. A. Vaia, *Nat. Mater.* **2004**, *3*, 115.
[60] A. Lendlein, H. Y. Jiang, O. Junger, R. Langer, *Nature* **2005**, *434*, 879.
[61] A. Lendlein, S. Kelch, *Angew. Chem., Int. Ed.* **2002**, *41*, 2034.
[62] Y. Shi, M. Yoonessi, R. A. Weiss, *Macromolecules* **2013**, *46*, 4160.
[63] J. A. Shumaker, A. J. W. McClung, J. W. Baur, *Polymer* **2012**, *53*, 4637.
[64] X. L. Xiao, D. Y. Kong, X. Y. Qiu, W. B. Zhang, F. H. Zhang, L. W. Liu, Y. J. Liu, S. Zhang, Y. Hu, J. S. Leng, *Macromolecules* **2015**, *48*, 3582.
[65] X. L. Xiao, X. Y. Qiu, D. Y. Kong, W. B. Zhang, Y. J. Liu, J. S. Leng, *Soft Matter* **2016**, *12*, 5824.
[66] N. Zheng, G. Q. Fang, Z. L. Cao, Q. Zhao, T. Xie, *Polym. Chem.* **2015**, *6*, 3046.
[67] D. J. Maitland, M. F. Metzger, D. Schumann, A. Lee, T. S. Wilson, *Lasers Surg. Med.* **2002**, *30*, 1.
[68] Y. Liu, B. Shaw, M. D. Dickey, J. Genzer, *Sci. Adv.* **2017**, *3*, e1602417.
[69] M. J. Biercuk, M. C. Llaguno, M. Radosavljevic, J. K. Hyun, A. T. Johnson, J. E. Fischer, *Appl. Phys. Lett.* **2002**, *80*, 2767.
[70] Q. T. Zhang, J. Wommer, C. O'Rourke, J. Teitelman, Y. C. Tang, J. Robison, G. J. Lin, J. Yin, *Extreme Mech. Lett.* **2017**, *11*, 111.
[71] K. Yu, Q. Ge, H. J. Qi, *Nat. Commun.* **2014**, *5*, 3066.